Opportunities for the Integration of Solar Thermal Heat, Photovoltaics and Biomass in a Brazilian Hospital

Eduardo A. Pina, Miguel A. Lozano, Luis M. Serra

GITSE-I3A, Department of Mechanical Engineering, University of Zaragoza, Zaragoza (Spain)

Abstract

The present study assesses the technical, economic and environmental feasibility of integrating renewable energy technologies (photovoltaic panels, solar thermal collectors, and biomass boilers), thermal energy storage units, absorption chillers, mechanical chillers, natural gas boilers, and power exchange with the grid in a university hospital located in Campinas (Brazil). The proposed design procedure combines mathematical programming techniques, such as a mixed integer linear programming model, addressing the synthesis, operational planning and dynamic operation conditions, with process integration techniques, such as the problem table algorithm (the algebraic tool of Pinch Analysis). The methodology is applied considering actual local data (energy demands, energy prices, climatic data), investment costs, and CO_2 emissions factors. The results show that under the conditions considered herein, biomass is economically the most appropriate fuel for heat production, displacing the deployment of natural gas; cooling production, on the other hand, is made entirely with electricity purchased from the grid. From the solar energy technologies, only the photovoltaic panels were included as a result of the condition that the annual electricity sold to the grid must be equal to the annual electricity purchased.

Keywords: Biomass, CSP, energy storage, optimization, photovoltaics, renewable energy, solar thermal.

1. Introduction

Renewable energy sources (RES), along with high-efficiency cogeneration systems, play a fundamental role in the transition towards sustainable energy systems. Renewable energy technologies (RETs) based on solar (e.g. photovoltaic and solar thermal collectors), wind (e.g. wind turbine generator), and biomass (e.g. biomass boiler) resources, among others, can be used to cover multiple energy demands directly, such as solar heat for space heating, and/or effectively coupled to heating/cooling technologies, such as solar heat to drive an absorption chiller. These systems, in which two or more energy services are produced from common resources, may be referred to as polygeneration systems. Owing to an appropriate energy integration between the constituting devices, polygeneration systems can achieve higher energy efficiency, lower primary energy consumption, lower unit costs of the final products, and lower environmental burdens relative to the conventional separate production (Mancarella, 2014; Rong and Lahdelma, 2016; Serra et al., 2009).

Despite having been applied in the industrial sector for decades, there is still very limited deployment of polygeneration systems in the buildings sector. Hospitals are great candidates for the application of such systems due to their long operating hours, regular occupation, large amounts of thermal energy required, and varied energy services demand, which typically include electricity, steam, space heating, domestic hot water, and chilled water (Biglia et al., 2017; Santo, 2014; Gimelli and Muccillo, 2013; Lozano et al., 2009). The multi-faceted nature of polygeneration systems (multiple energy resources, multiple energy products, multiple technology options) requires a design procedure that provides flexible, efficient and reliable energy systems. The design is further complicated as new factors are taken into account, such as the normative for power exchange with the electric grid, the decreasing investment costs of photovoltaic panels and solar thermal collectors, subsidies to the deployment of renewables, and the increased opportunity for biomass.

In this regard, mathematical optimization techniques based on mixed integer linear programming (MILP) models are suitable tools to address the synthesis (installed technologies and capacities, etc.) and operational planning (strategy concerning the operational state of the equipment, energy flow rates, purchase/selling of electricity, etc.) of polygeneration systems, as well as dynamic operation conditions, such as the intermittent behavior of solar resource, daily and annual fluctuations in energy demands and energy prices, interactions with the electric grid.

doi:10.18086/eurosun2018.05.03 Available at http://proceedings.ises.org

The issue is that, in general, studies have considered fixed layouts for the heat recovery between the equipment supplying and demanding heat. As a result, there is a thermodynamic oversimplification in which both the heat flow's temperature and use are set before the optimization procedure even begins.

In a previous paper (Pina et al., 2018), we have proposed a first approach to this problem by introducing in the superstructure a heat integration subsystem, in which the hot flows supplied by generation technologies (e.g. natural gas boilers) and the cold flows associated with technologies that produce energy services (e.g. absorption chillers, domestic hot water network) can be integrated through a virtual heat exchangers network, providing flexibility for the model to optimally couple the heat offer and demand in both quantity and quality (temperature). Thus, the Pinch Analysis, by means of the problem table algorithm, and mathematical programming, based on a MILP model, were combined to achieve a more realistic and efficient process integration. The methodology was applied to a university hospital located in Campinas (Brazil), demonstrating that cogeneration was by far the most economically interesting option to attend the hospital's energy demands; solar energy technologies, however, were only included under highly advantageous conditions.

Therefore, the present study continues the work started in the previous paper, aiming at a 100% renewable energy system. To this end, cogeneration was removed from the previous model and biomass was introduced, along with additional RETs (parabolic trough concentrators and biomass boilers). Also, the environmental impacts of installing and operating the system were assessed through the CO_2 emissions factors. The improved optimization model is applied to the same university hospital as considered in Pina et al. (2018), evaluating the technical, economic, and environmental feasibility of integrating RETs, thermal energy storage (TES) units, thermally activated technologies (TATs), mechanical chillers, natural gas boilers, and power exchange with the electric grid.

2. Renewable-based energy system

The synthesis of energy systems begins with the definition of the superstructure (Iyer and Grossmann, 1998; Lozano et al., 2010; Yokoyama et al., 2015). The first step in defining the superstructure is to identify the design targets, which correspond to the types and quantities of the energy demands of the consumer center and the energy resources available. Then, the superstructure can be established, considering potential technologies and the feasible connections between them, based on appropriate process integration. Once the superstructure is defined, additional and more specific data must be collected and elaborated, including technical, economic, and environmental data. This step plays an essential role in the synthesis problem since the quality of the data used directly affects the validity of the results of the optimization model. These steps are described in the following subsections.

2.1. Consumer center's energy demands

The consumer center considered herein corresponds to a medium size university hospital with 65,000 m² constructed area located in the city of Campinas (latitude -22.9º), Brazil. The hospital's energy demands consist of electricity, steam (saturated steam, 180 ºC), hot water (60 ºC), and chilled water (7 ºC). It should be noted that the electricity demand accounts for lighting, elevators and other devices, thus excluding the consumption for thermal energy production (e.g. electricity consumption to produce cooling). The energy demands are assumed to be known beforehand, their values have been originally presented by Santo (Santo, 2014).

Local climatic data for Campinas was obtained from the software METEONORM (METEOTEST, 2018). These data include the hourly ambient temperature T_a, hourly global solar radiation on a surface tilted 20º facing north Q_r, and hourly normal direct solar radiation Q_{Bn}.

The analysis has been carried out for the period of one year, which is divided into 24 representative days *d* (one working day *wd* and one weekend/holiday *we* for each month of the year), each one composed of 24 consecutive periods *h* of 1-hour duration. Table 1 shows the number of representative days type *d* per year *NRY*.

Table 1: Number of representative days type *d* per year *NRY*

Day	Jan	Feb	Mar	Apr	May	Jun	Jul	Aug	Sep	Oct	Nov	Dec
wd	21	19	22	20	20	21	23	21	21	21	19	22
we	10	9	9	10	11	9	8	10	9	10	11	9

The annual energy demands of the hospital are: electricity 9,633.5 MWh, hot water 518.7 MWh, steam 4,660.3 MWh, and chilled water 4,755.7 MWh. Table 2 shows the hospital's daily energy demands grouped by the season of the year. An example is provided in Figure 1, which depicts the hourly energy demands for a working day in January (summer, maximum electricity and cooling demands) and in July (winter, maximum hot water demand).

Table 2: Hospital's daily energy demands, kWh/day

Energy demand	Summer (Jan-Mar)		Autumn (Apr-Jun)		Winter (Jul-Sep)		Spring (Oct-Dec)	
	wd	*we*	*wd*	*we*	*wd*	*we*	*wd*	*we*
Electricity E_d	31,614	25,503	27,262	21,384	25,375	20,840	28,273	22,996
Steam V_d	16,257	15,037	10,947	11,858	10,393	12,868	12,236	14,206
Hot water Q_d	1,178	889	1,788	1,077	2,039	1,225	1,438	822
Chilled water R_d	18,321	16,412	12,116	11,580	8,424	7,896	14,788	13,205

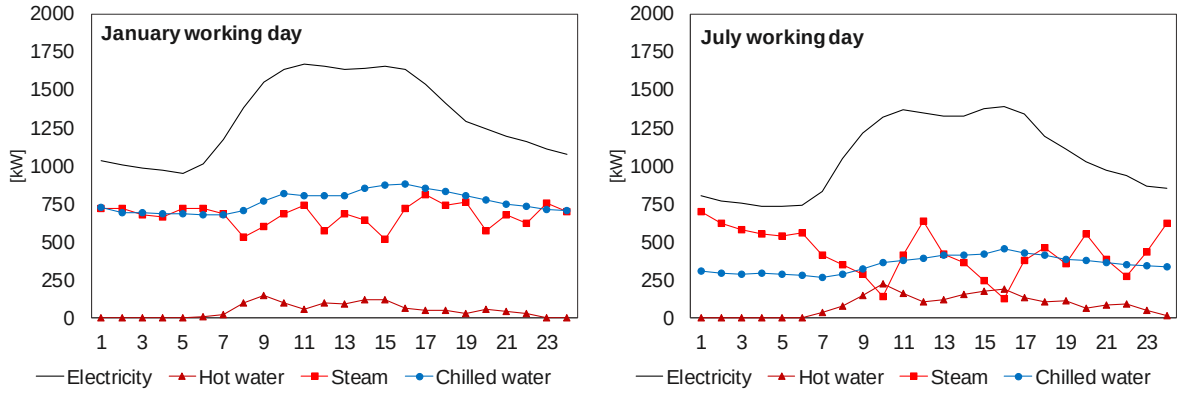

Figure 1: Hourly energy demands for a representative working day in January (left) and July (right)

2.2. Superstructure and thermal integration subsystem

The superstructure of the renewable-based energy system is depicted in Figure 2. The energy resources available to the system include both renewable (solar radiation and biomass) and conventional (natural gas and electricity purchased from the grid) resources. The energy system must attend the consumer center's energy demands, namely electricity E_d, steam V_d, hot water Q_d, and chilled water R_d. It is considered that a part of the electricity produced by the system can be sold to the grid. Also, an auxiliary electricity consumption was considered for most of the candidate technologies.

The candidate technologies in the superstructure can be divided into three groups:

- Generation: These technologies convert the energy resource into intermediate or final products. When the technology consumes a renewable energy resource, it may be referred to as a RET. Considering the energy resource's availability, the generation technologies may be classified as dispatchable (biomass hot water boiler BH, biomass steam boiler BV, natural gas hot water boiler GH, and natural gas steam boiler GV) and non-dispatchable or intermittent (photovoltaic panel PV, flat-plate solar thermal collector ST, and parabolic trough concentrator PT);
- Transformation: These technologies convert an energy product into a different one. The transformation technologies in the superstructure are the electric chiller EC, the single-effect absorption chiller AS, and the double-effect absorption chiller AD;
- Storage: These technologies store the energy product for later use. A hot water storage tank HS and a chilled water storage tank CS have been included in the superstructure.

The only exception to this classification is the cooling tower CT, which is a heat rejection technology that must be installed to dissipate to the ambient air the heat from the transformation technologies and from the thermal integration subsystem.

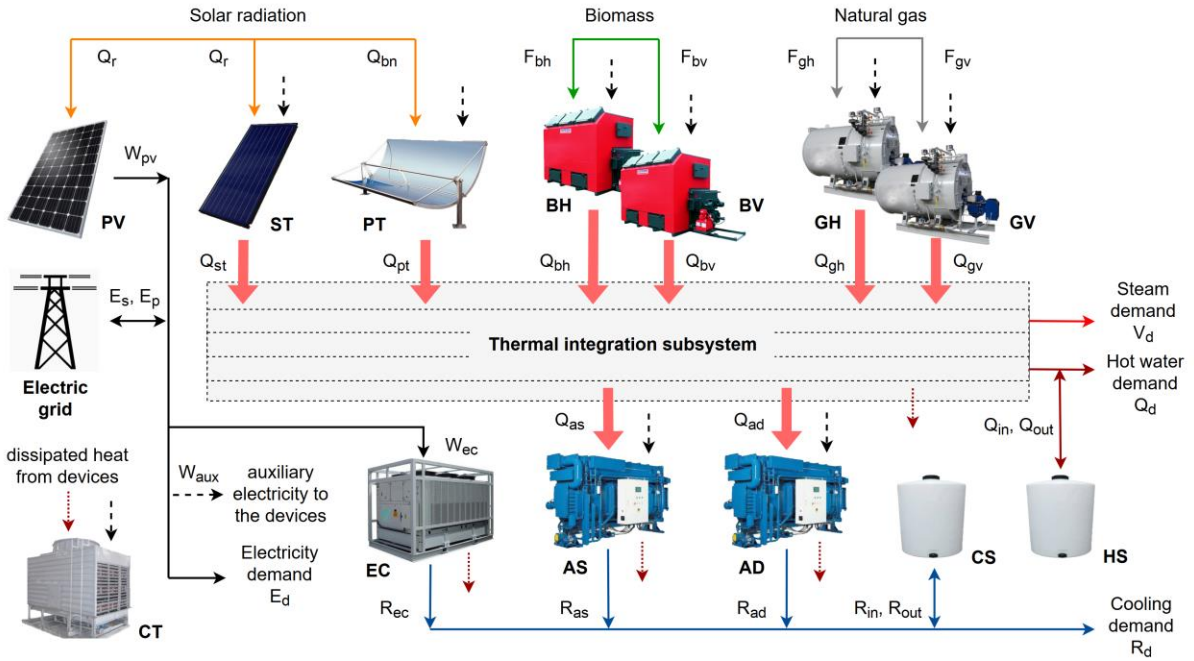

Figure 2: Superstructure of the renewable-based energy system

An appropriate thermal integration requires that the thermal energy flows be evaluated in terms of quantity (kWh produced) and quality (temperature levels). In this regard, Figure 3 (a) shows the thermal integration of the hot and cold flows in the energy system (Figure 2), providing their initial (supply) and final (target) temperatures, and the unit flow production or consumption in kg/s per MW of operating capacity; six temperature intervals were identified, the first being the hottest. The heat balance in a general temperature interval *k* is shown in Figure 3 (b).

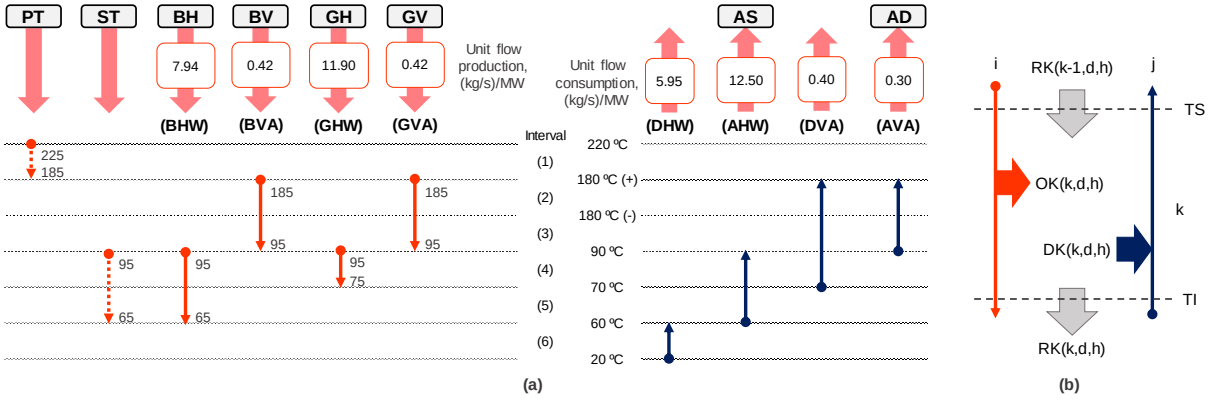

Figure 3: (a) Thermal integration subsystem, and (b) heat balance in a general temperature interval *k*

Originally introduced in a previous paper (Pina et al., 2018), the superstructure's thermal integration subsystem connects the generation technologies to the transformation technologies and to the steam and hot water energy demands. In other words, it serves as interface between the heat supply and the heat demand through a virtual network of heat exchangers. The generation technologies are associated with the following hot flows: (i) the BH supplies hot water Q_{bh} at 95 ºC from hot water at 65 ºC (flow BHW); (ii) the BV supplies saturated steam Q_{bv} at 185 ºC from hot water at 95 ºC (flow BVA); (iii) the GH supplies hot water Q_{gh} at 95 ºC from hot water at 75 ºC (flow GHW); (iv) the GV supplies saturated steam Q_{gv} at 185 ºC from hot water at 95 ºC (flow GVA); (v) the PT supplies heat Q_{pt} directly into the first (hottest) temperature interval; and (vi) the ST supplies heat Q_{st} directly into the fourth temperature level. The transformation technologies are associated with the following cold flows: (i) the AS produces chilled water R_{as} at 7 ºC, consuming hot water at 90 ºC and discharging it at 60 ºC (flow AHW); and (ii) the AD produces chilled water R_{ad} at 7 ºC, consuming saturated steam at 180 ºC and discharging hot water at 90 ºC (flow AVA). Cold flows can also be directly related to the energy demands: steam V_d at 180 ºC returning as hot water at 70 ºC (flow DVA), and hot water Q_d at 60 ºC returning at 20 ºC (flow DHW). The minimum temperature difference of 5 ºC was adopted in the thermal integration subsystem.

2.3. Data collection and elaboration

All candidate technologies included in the superstructure (Figure 2) are commercially available. The technologies can modulate up to nominal load, except for the intermittent RETs (PV, PT, and ST). Table 3 presents the main technical, economic, and environmental parameters of the technologies, obtained from the manufacturers' catalogues and from the literature. The unit auxiliary electricity consumption *cue* is given per unit of operation capacity, while the bare module cost *CI* and the unit CO_2 emissions *CO2U* are given per unit of installed capacity. It is assumed that no energy losses take place in the TES units ($\eta_{TES} = 1$).

Table 3: Technical, economic, and environmental parameters of the technologies in the superstructure

Technology *t*	**Technical parameters**	**Unit electricity consumption *cue* kW_{el}/kW**	**Bare module cost *CI* €/kW_{nom}**	**Unit CO_2 emissions *CO2U* kg CO_2/kW_{nom}**
PV	P_{pv} = 0.34 kWp, $A_{m,pv}$ = 1.94 m², *RapPV* = 5.707 m²/kWp, η_{pv} = 0.1752, μ_T = 0.0038 °C^{-1}	-	1300	1840
ST	$A_{m,st}$ = 12 m², *RapST* = 1.4286 m²/kWp, η_0 = 0.806, k_1 = 2.580 W/(m²·K), k_2 = 0.009 W/(m²·K²)	0.0050	500	140
PT	*RapPT* = 1.5172 m²/kW	0.0164	425	130
BH	$\eta_{bh} = Q_{bh}/F_{bh}$ = 0.85	0.0050	310	15
BV	$\eta_{bv} = Q_{bv}/F_{bv}$ = 0.85	0.0050	375	20
GH	$\eta_{gh} = Q_{gh}/F_{gh}$ = 0.92	0.0050	55	10
GV	$\eta_{gv} = Q_{gv}/F_{gv}$ = 0.93	0.0050	120	10
AS	$COP_{as} = R_{as}/Q_{as}$ = 0.635	0.0050	260	165
AD	$COP_{ad} = R_{ad}/Q_{ad}$ = 1.41	0.0050	260	165
EC	$COP_{ec} = R_{ec}/Q_{ec}$ = 6.11	-	105	160
CT	η_{ct} = 1	0.0050	30	25
HS	η_{TES} = 1	-	40	150
CS	η_{TES} = 1	-	80	300

The PT has been modeled using the System Advisor Model (SAM) (NREL, 2018). The SAM is a free software package which contains hourly performance and economic models for concentrating solar power (CSP) systems, photovoltaic, solar hot-water, and generic fuel-use technologies. An in-depth explanation of the model can be found in Wagner and Gilman (2011). Only a few key parameters have been changed in the basic model, leaving the rest with their default values. The considerations were the following: On the model's first page, *Location and Resource*, METEONORM's weather file for Campinas was imported; *System Design* is the model's second page, in which the system's nominal ratings are defined; it was considered that (i) the direct normal irradiance available at design point was equal to 950 W/m²; (ii) the target solar multiple (ratio of the target receiver thermal power and heat sink power) was equal to 1; (iii) the loop inlet and outlet heat transfer fluid (HTF) temperatures were 185 and 225 °C, respectively; (iv) the heat sink power was equal to 1.5 MWth; and (v) the hours of storage at design point were zero. Following to the next page, *Solar Field*, it was necessary to choose a different HTF to match the operation temperatures previously set; thus, the Downtherm RP field HTF fluid was selected. Finally, on the next two pages, *Collectors (SCAs)* and *Receivers (HCEs)*, the collector SkyFuel SkyTrough and the receiver Schott PTR80 were chosen from their respective libraries.

From the model's results, the following data are given as input to the optimization model developed herein: (i) the area to power ratio *RapPT* of 1.5172 m²/kW; and (ii) the unit production per m² installed of PT, $x_{pt}(d,h)$, for each hourly period *h* of each representative day *d*.

The bare module costs *CI* in Table 3 were obtained from various references: Guadalfajara (2016), IEA (2017), Kurup and Turchi (2015), Lazard (2016), and Ramos (2012). The *CI* is the purchase cost multiplied by a simple module factor, which accounts for transportation, installation, connection costs, etc. Additional economic data include the amortization and maintenance factor *fam*, equal to 0.15 yr^{-1}, and the indirect costs factor *fic*, equal to 0.20 (Ramos, 2012). The plant's operational lifetime *nyr* was considered to be 20 years.

Regarding the unit CO_2 emissions values *CO2U* in Table 3, they were obtained from Burkhardt et al. (2011), Carvalho (2011), Guadalfajara (2016), Ito et al. (2009), Raluy et al. (2014), and WEC (2016).

Local energy prices are required for the assessment of the system's annual operation cost: (i) the natural gas purchase price is *pgncon* = 0.035 €/kWh (LHV) (COMGAS, 2018); (ii) the purchase price of the pellets is *pcebio* = 0.026 €/kWh (LHV) (Delgado et al., 2018); and (iii) two billing periods apply for the electricity: on-peak tariff *pcepta* = 0.136 €/kWh (between hours 18 and 20 from March to October and hours 19 and 21 for the remaining months) and off-peak tariff *pcevle* = 0.094 €/kWh (for the rest of the hours of the year) (CPFL, 2018); additionally, the electricity selling price was assumed to be the purchase price at the corresponding hour minus a penalization of *penven* = 0.012 €/kWh.

In terms of CO_2 emissions, the environmental impact associated with the consumption of energy resources is assessed through: (i) the natural gas emission factor $kgCO2_{con}$ = 0.2020 kg CO_2/kWh (Rupp and Lamberts, 2017); (ii) the pellets emission factor $kgCO2_{bio}$ = 0.0506 kg CO_2/kWh (Delgado et al., 2018); and (iii) the emission factor of the electricity available in the national electric grid *kgCO2e*, which varies hourly and daily. The hourly $kgCO2_e$ are available for the whole year in (MCTIC, 2018); for the present study, we have processed the data for 2016 to obtain the average hourly CO_2 emissions for each representative day *d*. The annual average is 0.6228 kg CO_2/kWh.

3. Mathematical model

A MILP model was developed to determine the optimal cost configuration and operational planning of the renewable-based energy system analyzed herein. The model is composed of decision variables representing: (i) the existence and size of the technologies; (ii) the operation load of each technology in each time interval; (iii) the energy resources exchanged with the economic market (electricity, natural gas, and biomass) and the solar radiation; (iv) the capacity of the TES units and the corresponding energy stored in each time interval; (v) the heat supply and demand in each temperature interval; and (vi) the heat surplus from a temperature interval to the next (heat cascade). The existence of technologies and external (legal) restrictions, such as the permission to sell electricity to the grid, are represented by binary variables, while all other variables are continuous.

The objective function is explained in Section 3.1. The environmental aspects of installing and operating the system are incorporated in the model, as described in Section 3.2. Section 3.3 presents the methodology employed to determine the hourly productions per m² of PV and ST installed. Finally, Section 3.4. presents the model's constraints.

3.1. Objective function: Economic criterion

The objective function to be minimized is the total annual cost CTE_{tot}, which consists of the annual fixed cost CTE_{fix} and the annual variable cost CTE_{var}.

$$Min\ CTE_{tot} = CTE_{fix} + CTE_{var} \quad \text{(Eq. 1)}$$

The annual fixed cost is expressed by Eq. 2, where *PIN(t)* is the installed capacity of the technology *t*.

$$CTE_{fix} = fam \cdot (1 + fic) \cdot \sum_t CI(t) \cdot PIN(t) \quad \text{(Eq. 2)}$$

The annual variable cost CTE_{var} corresponds to the sum, for each hourly period *h* of each representative day *d*, of the costs of purchasing natural gas $CTE_{gas}(d,h)$, biomass $CTE_{bio}(d,h)$, and electricity $CTE_{ele}(d,h)$:

$$CTE_{var} = \sum_{d,h} NRY(d) \cdot \left(CTE_{gas}(d,h) + CTE_{bio}(d,h) + CTE_{ele}(d,h)\right) \quad \text{(Eq. 3)}$$

$$CTE_{gas}(d,h) = pgncon \cdot \left(F_{gh}(d,h) + F_{gv}(d,h)\right) \quad \text{(Eq. 4)}$$

$$CTE_{bio}(d,h) = pcebio \cdot \left(F_{bh}(d,h) + F_{bv}(d,h)\right) \quad \text{(Eq. 5)}$$

$$CTE_{ele}(d,h) = pelcom(d,h) \cdot E_p(d,h) - pelven(d,h) \cdot E_s(d,h) \quad \text{(Eq. 6)}$$

where, in each time interval, *pelcom(d,h)* is the electricity purchase price (on-peak *pcepta* or off-peak *pcevle*, as defined in Section 2.3) and *pelven(d,h)* is the electricity selling price (purchase price *pelcom(d,h)* minus the penalization *penven* defined in Section 2.3).

3.2. Environmental criterion

Analogous to the economic criterion (objective function), the total annual CO_2 emissions $CO2_{tot}$ consists of the annual fixed emissions $CO2_{fix}$ and the annual variable emissions $CO2_{var}$.

$$CO2_{tot} = CO2_{fix} + CO2_{var} \quad \text{(Eq. 7)}$$

The $CO2_{fix}$, annualized over the plant's operational lifetime *nyr* is expressed by Eq. 8.

$$CO2_{fix} = \sum_{t} CO2U(t) \cdot PIN(t)/nyr \quad \text{(Eq. 8)}$$

The $CO2_{var}$ consists of the terms relative to the consumption of natural gas $CO2_{gas}(d,h)$, biomass $CO2_{bio}(d,h)$, and electricity $CO2_{ele}(d,h)$:

$$CO2_{var} = \sum_{d,h} NRY(d) \cdot \left(CO2_{gas}(d,h) + CO2_{bio}(d,h) + CO2_{ele}(d,h)\right) \quad \text{(Eq. 9)}$$

$$CO2_{gas}(d,h) = kgCO2con \cdot \left(F_{gh}(d,h) + F_{gv}(d,h)\right) \quad \text{(Eq. 10)}$$

$$CO2_{bio}(d,h) = kgCO2bio \cdot \left(F_{bh}(d,h) + F_{bv}(d,h)\right) \quad \text{(Eq. 11)}$$

$$CO2_{ele}(d,h) = kgCO2e(d,h) \cdot \left(E_p(d,h) - E_s(d,h)\right) \quad \text{(Eq. 12)}$$

3.3. PV and ST solar productions

The performances of the solar technologies are dependent on the local climatic conditions, which vary hourly and daily. Taking the climatic data for the city of Campinas, obtained from METEONORM as explained in Section 2.1, and the technical parameters given in Table 3, the unit production per m² of installed PV and ST were calculated. As explained in Section 2.3, the unit production per m² of PT was obtained through the SAM software.

For each hourly period *h* of each representative day *d*, the unit electricity production per m² of PV installed $x_{pv}(d,h)$ is determined by Eq. 13, according to the methodology by Duffie et al. (2013). The maximum power P_{pv}, surface area $A_{m,pv}$, module efficiency η_{pv}, and temperature coefficient of power μ_T are given in Table 3. Irradiation and cell temperature at SRC conditions are $Q_{r,SRC}$ = 1 kW/m² and $T_{c,SRC}$ = 25 ºC, respectively. Irradiation, cell temperature and ambient temperature at NOCT conditions are $Q_{r,NOCT}$ = 0.8 kW/m², $T_{c,NOCT}$ = 45 ºC and $T_{a,NOCT}$ = 20 ºC, respectively. The efficiency of power-conditioning equipment η_e = 0.9. The hourly cell temperature $T_{c,pv}(d,h)$ and the hourly temperature correction factor $F_{top}(d,h)$ are obtained by solving Eqs. 14 and 15.

$$x_{pv}(d,h) = \frac{P_{pv}}{A_{m,pv}} \cdot \frac{Q_r(d,h)}{Q_{r,SRC}} \cdot F_{top}(d,h) \cdot \eta_e \quad \text{(Eq. 13)}$$

$$F_{top}(d,h) = 1 - \mu_T \cdot \left(T_{c,pv}(d,h) - T_{c,SRC}\right) \quad \text{(Eq. 14)}$$

$$T_{c,pv}(d,h) = T_a(d,h) + \left(T_{c,NOCT} - T_{a,NOCT}\right) \cdot \frac{Q_r(d,h)}{Q_{r,NOCT}} \cdot \left(1 - \frac{\eta_{pv} \cdot F_{top}(d,h)}{0.9}\right) \quad \text{(Eq. 15)}$$

The unit production per m² of ST collector $x_{st}(d,h)$ is calculated by Eq. 16, in which the performance coefficients k_0, k_1 and k_2 are found in Table 3, and ΔT is the temperature difference between the collector $T_{c,st}$ = 95 ºC and the ambient $T_a(d,h)$, according to Eq. 17. Only the positive values of collected heat are considered.

$$x_{st}(d,h) = Max(k_0 \cdot Q_r(d,h) - k_1 \cdot \Delta T(d,h) - k_2 \cdot \Delta T(d,h)^2; 0) \quad \text{(Eq. 16)}$$

$$\Delta T(d,h) = T_{c,st} - T_a(d,h) \quad \text{(Eq. 17)}$$

3.4. Model constraints

The objective function is subject to the following types of constraints:

(i) Equipment constraints: Include capacity limits and production restrictions for each technology *t*. Capacity limits are inequality constraints that limit the installed capacity *PIN(t)* to the maximum installable capacity $PIN_{MAX}(t)$. The binary variable *YINS(t)* expresses the permission to install the technology *t*.

$$PIN(t) \leq YINS(t) \cdot PIN_{MAX}(t) \quad \text{(Eq. 18)}$$

Production restrictions limit the production of a technology *t* to its installed capacity and relate the technology's energy consumption to its production. An example is provided herein for the flat-plate solar thermal collector ST:

$$Q_{st}(d,h) \leq x_{st}(d,h) \cdot RapST \cdot PIN(ST) \quad \text{(Eq. 19)}$$

An auxiliary electricity consumption has been considered for most technologies. For example, the BV auxiliary electricity consumption $W_{aux,bv}(d,h)$ is calculated according to Eq. 20.

$$W_{aux,bv}(d,h) = cue(BV) \cdot Q_{bv}(d,h) \quad \text{(Eq. 20)}$$

(ii) Energy balances: For each energy service, in each time interval. Taking the electricity as an example, in each time interval, the following energy balance must hold true:

$$E_p(d,h) + W_{pv}(d,h) = E_d(d,h) + E_s(d,h) + W_{ec}(d,h) + W_{aux}(d,h) \quad \text{(Eq. 21)}$$

(iii) Electric grid constraints: A binary variable is used to express the permission to sell electricity to the grid.

(iv) Thermal integration constraints: As explained in Pina et al. (2018), the heat cascade depicted in Figure 3 (a) has been modeled based on the transshipment model of Papoulias and Grossmann (1983). As explained in Section 2.2, temperature intervals *k* were defined, in which hot *i* and cold *j* flows exchange heat. The heat balance in each temperature interval and time interval is expressed by Eq. 23, in accordance with Figure 3 (b).

$$RK(k,d,h) + DK(k,d,h) = RK(k-1,d,h) + OK(k,d,h) \quad \text{(Eq. 22)}$$

where $RK(k,d,h)$ is the surplus heat of the temperature interval *k*, $RK(k\text{-}1,d,h)$ is the surplus heat from the previous temperature interval *k-1*, $OK(k,d,h)$ is the heat supplied by the hot flows *QIK* plus the ST and PT solar heat (Eq. 23) and $DK(k,d,h)$ is the heat consumed by the cold flows *QJK* (Eq. 24). The fundamental requirement of the Second Law of Thermodynamics is that $RK(k) \geq 0$.

$$OK(k,d,h) = YSK(k) \cdot Q_{st}(d,h) + YPK(k) \cdot Q_{pt}(d,h) + \sum_i QIK(i,k,d,h) \quad \text{(Eq. 23)}$$

$$DK(k,d,h) = \sum_j QJK(j,k,d,h) \quad \text{(Eq. 24)}$$

As explained in Section 2.3, the ST and the PT supply heat directly into the corresponding temperature interval; this is done through the binary variables *YSK(k)* and *YPK(k)*, which express the temperature interval in which the solar heat $Q_{st}(d,h)$ and $Q_{pt}(d,h)$ are delivered, respectively.

For each time interval, each of the thermal flows entering (Q_{st}, Q_{pt}, Q_{bh}, Q_{bv}, Q_{gh}, Q_{gv}) and leaving ($Q_d + Q_{in} - Q_{out}$, V_d, Q_{as}, Q_{ad}) the thermal integration subsystem (Figure 2 and Figure 3 (a)) can be determined as the sum of the total heat supplied or demanded throughout the temperature intervals. An example is provided below for the BH:

$$Q_{bh}(d,h) = \sum_k QIK(BHW,k,d,h) \quad \text{(Eq. 25)}$$

4. Results

The optimization model has been solved using the software LINGO (Schrage, 1999). Different system configurations have been evaluated considering different structural and operational conditions. Structural conditions involved the permission to install the candidate technologies from the superstructure depicted in Figure 2, while operational conditions concerned the different approaches to the interconnection with the electric grid.

First, the reference system (Configuration A) was obtained by removing the permission to install the RETs and TES units. The optimal economic cost solution (Configuration B) was then evaluated, in which all candidate technologies could be installed, and the system could purchase as much electricity from the grid as necessary. Based on the optimal economic solution, an additional system configuration (Configuration C) was obtained by imposing the condition of a zero annual balance with the electric grid (throughout the year, the system must inject back into the electric grid the same amount of purchased electricity). The main results obtained for each system are shown in Table 4 and Table 5. Moreover, the configuration and annual energy flows of the reference and optimal economic cost configurations are depicted in Figure 4; the thermally integrated technologies are found enclosed in the dashed line.

Table 4: Installed technologies in the reference and optimal economic configurations.

Technology	Configuration A			Configuration B			Configuration C		
	***PIN*, kW**	**Investment, €**	***fu*, %**	***PIN*, kW**	**Investment, €**	***fu*, %**	***PIN*, kW**	**Investment, €**	***fu*, %**
PV	x	x	x	0	0	0	6,344	9,896,792	18.8
ST	x	x	x	0	0	0	0	0	0
PT	x	x	x	0	0	0	0	0	0
BH	x	x	x	0	0	0	0	0	0
BV	x	x	x	533	239,714	96.7	533	239,714	96.7
GH	76	5,047	1.6	27	1,808	2.0	27	1,808	2.0
GV	780	112,356	75.6	248	35,648	30.6	248	35,648	30.6
AS	0	0	0	0	0	0	0	0	0
AD	0	0	0	0	0	0	0	0	0
EC	879	110,781	61.7	871	109,726	62.3	854	107,616	63.6
CT	1,023	36,833	61.7	1,013	36,482	62.3	994	35,781	63.6
HS, kWh	x	x	x	49	2,356	-	49	2,356	-
CS, kWh	x	x	x	8	804	-	42	4,019	-

Table 5: Main results for the reference and optimal economic configurations.

	Configuration A	Configuration B	Configuration C
Natural gas, MWh/yr	5,567	719	719
Biomass, MWh/yr	0	5,304	5,304
Purchased electricity, MWh/yr	10,466	10,466	5,215
Sold electricity, MWh/yr	0	0	5,215
Natural gas, €/yr	194,851	25,152	25,152
Biomass, €/yr	0	137,904	137,904
Purchased electricity, €/yr	1,021,641	1,021,626	527,973
Sold electricity, €/yr	0	0	427,603
Annual variable cost, €/yr	1,216,492	1,184,682	263,425
Annual fixed cost, €/yr	39,753	63,981	1,548,560
Total annual cost, €/yr	1,256,245	1,248,662	1,811,985
Investment cost, €	265,017	426,537	10,323,732
Natural gas, kg CO_2/yr	1,124,568	145,164	145,164
Biomass, kg CO_2/yr	0	268,223	268,223
Purchased electricity, kg CO_2/yr	6,508,147	6,508,152	3,254,982
Sold electricity, kg CO_2/yr	0	0	3,239,618
Annual variable CO_2 emissions, kg CO_2/yr	7,632,715	6,921,540	428,752
Annual fixed CO_2 emissions, kg CO_2/yr	8,741	9,397	593,398
Total annual CO_2 emissions, kg CO_2/yr	7,641,456	6,930,937	1,022,150

As can be seen from Table 4, the only technologies installed in the reference system (Configuration A) include hot water GH and steam GV natural gas boilers, the electric chiller EC, and the cooling tower CT. The GV operates with a high load factor (75.6%), while the GH only covers occasional heat peak demands; in fact, the GH is virtually irrelevant to the system as it only covers 0.2% of the total annual heat production. In the case of the Configuration B, there is a shift from natural gas to biomass: a biomass steam boiler BV is installed to the detriment of the GV and GH, whose capacities are reduced by 65%. The BV operates with a very high load factor reaching the 97% figure, while the GV is responsible for covering heat peak demands (load factor 30.6%). By contrast, the cooling production remains entirely based on electricity from the electric grid in the EC. Even though this solution includes a hot water HS and a chilled water CS storage tanks, their capacities are extremely low. Configuration C is practically equal to the optimal economic cost, however with 6,344 kW of photovoltaic panels PV. It should be mentioned that the PV load factor has been calculated considering its nominal module power and whole year operation.

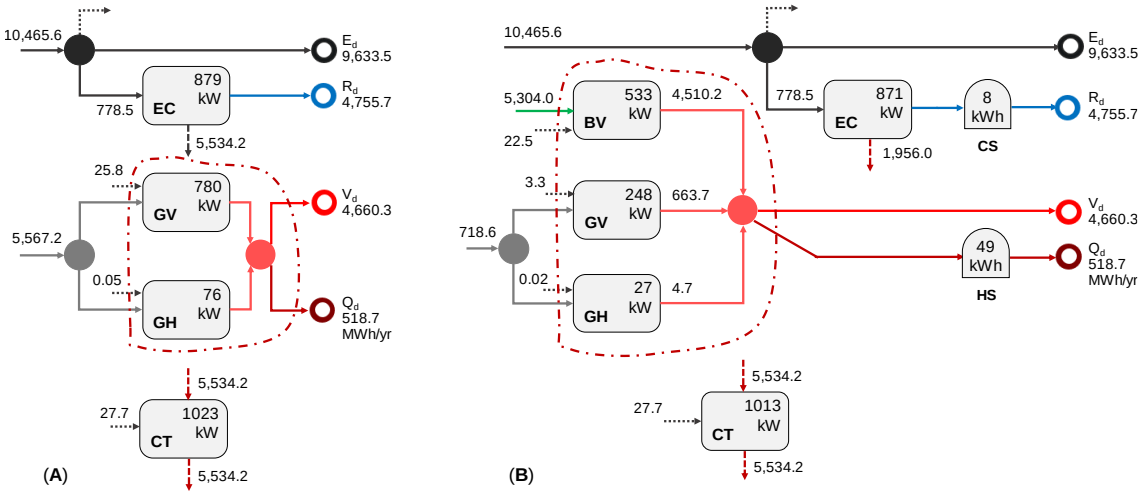

Figure 4: Configurations A and B with annual energy flows in MWh.

The results presented in Table 5 show that Configuration B has a total annual cost only 0.6% smaller than Configuration A; the fixed and the variable terms, on the other hand, are not the same: the annual installation and amortization cost in the optimal economic cost solution is about 61% higher than that of the reference system, while the annual variable cost is 2.6% lower. The increased investment cost (ΔInv = 426,537 - 265,017 = 161,520 €) is compensated by a reduction in the annual variable costs (ΔCTE_{var} = 1,216,492 – 1,184,682 = 31,810 €/yr), thus resulting in a Payback Period of 5 years. Regarding the total annual CO_2 emissions, Configuration B achieves a 9% reduction in the total annual CO_2 emissions relative to Configuration A; this is due to: (i) the shift from natural gas to biomass, which allowed the CO_2 emissions associated with the thermal energy production to be reduced from 1,124 tCO_2/yr to 413 tCO_2/yr; and (ii) the increase in the annual fixed CO_2 emissions from 8.7 to 9.4 tCO_2/yr.

The obligation to compensate, throughout the year, every kWh of purchased electricity with another kWh of sold electricity results in the installation of 6,344 kW of PV in Configuration C. This has a twofold effect: On the one hand, there is a dramatic increase in the investment cost of the system from 426,537 € to 10,323,732 €, 96% of which is attributed to the PV; on the other hand, the annual operation costs are sharply reduced by 78%, as now the system buys only a half of the electricity consumed (5,215 MWh/yr) and is able to sell the same amount, generating an income of 427,603 €/yr. As a consequence, the total annual cost of Configuration C is 45% higher than that of the Configuration B, with a Payback Period of 11 years. By contrast, the total annual CO_2 emissions are drastically reduced (86%), as the annual operation CO_2 emissions drop by 92%, compensating the increase in the emissions relative to the manufacturing of the PV.

Based on the previously discussed Configurations, removing the permission to install natural gas boilers in Configurations B and C led to the no fossil fuels and the 100% renewable Configurations D and E, respectively. The total annual costs and total annual CO_2 emissions for all Configurations are shown in the graph of Figure 5. As can be seen, natural gas did not play a significant role in neither of the optimal solutions.

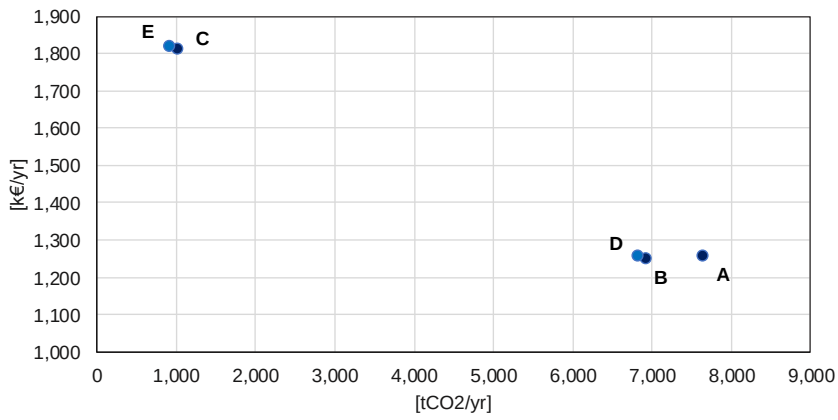

Figure 5: Total annual cost and total annual CO_2 emissions of different Configurations.

5. Conclusions

The present work was a follow-up to the previous study by Pina et al. (2018), in which a MILP model was developed to determine the optimal cost configuration and hourly operation strategy of a polygeneration system that must attend the energy demands of a Brazilian university hospital. Under the conditions considered in that study, it was evident from the results obtained that cogeneration gas engines were the most economically interesting option; consequently, the solar energy technologies, such as photovoltaic panels and solar thermal collectors, were never included in the optimal solutions except under highly advantageous conditions.

In order to continue in the direction of a 100% renewable energy system, it was proposed herein to improve the optimization model by: (i) removing the cogeneration gas engines altogether; (ii) incorporating an additional renewable energy resource, biomass, so that the system has both intermittent and dispatchable RES available; and (iii) providing RETs capable of producing thermal energy at higher temperature levels, such as the parabolic trough concentrators and the biomass steam boiler. The thermal integration subsystem originally introduced by Pina et al. (2018) was adjusted accordingly, thus allowing the optimization model to optimally match the heat supply and demand considering both quantity and quality (temperature). Moreover, the environmental aspects of installing and operating the energy system were taken into account in the improved optimization model.

In the present work, the results obtained for the case study of the Brazilian university hospital showed that biomass was economically the most appropriate fuel for heat production, displacing deployment of natural gas and reaching a share of 87% of the total thermal energy produced. The same cannot be said about the cooling production, which was made entirely with electricity purchased from the electric grid, thus proving that electricity was more appropriate for cooling production in the electric chiller than heat in the absorption chillers. Despite the shift from natural gas to biomass, the optimal economic system was rather similar to the reference system.

Solar energy technologies (both photovoltaic and solar thermal) remained elusive. Photovoltaic panels were only included when the system was required to achieve a zero annual balance with the electric grid. Thus, it would be interesting to carry out a sensitivity analysis to better understand the conditions in which these technologies become feasible in relation to other energy resources (e.g. natural gas and biomass) and to the interaction of the system with the electric grid. Likewise, it would be interesting to perform a sensitivity analysis concerning the use of absorption chillers for cooling production, as opposed to the mechanical chillers consuming electricity.

6. Acknowledgements

This work was developed in the frame of the research projects ENE2014-57262-R and ENE2017-87711-R, partially funded by the Spanish Government (Energy Program), the Government of Aragon (Spain) and the EU Social Fund (FEDER Program). Eduardo Pina acknowledges financial support from the Brazilian Federal Government and CNPq Science Without Borders Program.

7. References

Biglia, A., Caredda, F.V., Fabrizio, E., Filippi, M., Mandas, N., 2017. Technical-economic feasibility of CHP systems in large hospitals through the Energy Hub method: The case of Cagliari AOB. Energy Build. 147, 101–112. doi:10.1016/j.enbuild.2017.04.047.

Burkhardt, J.J., Heath, G.A., Turchi, C.S., 2011. Life cycle assessment of a parabolic trough concentrating solar power plant and the impacts of key design alternatives. Environ. Sci. Technol. 45, 2457–2464. doi:10.1021/es1033266.

Carvalho, M., 2011. Thermoeconomic and environmental analyses for the synthesis of polygeneration systems in the residential-commercial sector. PhD Thesis – University of Zaragoza. https://zaguan.unizar.es/record/5744/files/TESIS-2011-025.pdf (accessed 16.11.18).

COMGAS, 2018. Natural gas rates. https://www.comgas.com.br/tarifas/ (accessed 6.9.18).

CPFL, 2018. Electricity rates. CPFL Paul. https://www.cpflempresas.com.br/institucional/tarifas.aspx?emp=CPFL (accessed 6.9.18).

Delgado, D., Carvalho, M., Moreira, L., Junior, C., 2018. Analysis of Biomass-fired Boilers in a Polygeneration System for a Hospital. Front. Manag. Res. 2, 1–13. doi:10.22606/fmr.2018.21001.

Duffie, J.A., Beckman, W.A., Worek, W.M., 2013. Solar Engineering of Thermal Processes, 4th ed, Wiley. doi:10.1115/1.2930068.

Gimelli, A., Muccillo, M., 2013. Optimization criteria for cogeneration systems: Multi-objective approach and application in an hospital facility. Appl. Energy 104, 910–923. doi:10.1016/j.apenergy.2012.11.076.

Guadalfajara, M., 2016. Economic and environmental analysis of central solar heating plants with seasonal storage for the residential sector. PhD Thesis – University of Zaragoza. https://zaguan.unizar.es/record/56714/files/TESIS-2016-196.pdf (accessed 16.11.18).

IEA, 2017. District Energy Systems in China. https://www.iea.org/publications/freepublications/publication/DistrictEnergySystemsinChina.pdf (accessed 16.11.18).

Ito, M., Komoto, K., Kurokawa, K., 2009. A comparative LCA study on potential of very-large scale PV systems in Gobi desert. Conf. Rec. IEEE Photovolt. Spec. Conf. 000729–000732. doi:10.1109/PVSC.2009.5411180.

Iyer, R.R., Grossmann, I.E., 1998. Synthesis and operational planning of utility systems for multiperiod operation. Comput. Chem. Eng. 22, 979–993. doi:10.1016/S0098-1354(97)00270-6.

Kurup, P., Turchi, C.S., 2015. Parabolic Trough Collector Cost Update for the System Advisor Model (SAM). Tech. Rep. NREL/TP-6A20-65228 Natl. Renew. Energy Lab. 1–40. doi:10.2172/1227713.

LAZARD, 2016. Lazard's Levelized Cost of Energy Analysis 10.0, 1–21. https://www.lazard.com/media/438038/levelized-cost-of-energy-v100.pdf (accessed 16.11.18).

Lozano, M.A., Ramos, J.C., Carvalho, M., Serra, L.M., 2009. Structure optimization of energy supply systems in tertiary sector buildings. Energy Build. 41, 1063–1075. doi:10.1016/j.enbuild.2009.05.008.

Lozano, M.A., Ramos, J.C., Serra, L.M., 2010. Cost optimization of the design of CHCP (combined heat, cooling and power) systems under legal constraints. Energy 35, 794–805. doi:10.1016/j.energy.2009.08.022.

Mancarella, P., 2014. MES (multi-energy systems): An overview of concepts and evaluation models. Energy 65, 1–17. doi:10.1016/j.energy.2013.10.041.

MCTIC, 2018. Fatores de emissão da margem de operação pelo método da análise de despacho. http://www.mctic.gov.br/mctic/opencms/ciencia/SEPED/clima/textogeral/emissao_despacho.html (accessed 7.2.18) [In Portuguese].

METEOTEST, 2018. METEONORM. http://www.meteonorm.com/ (accessed 6.9.18).

NREL, 2018. System Advisor Model (SAM) . https://sam.nrel.gov/ (accessed 6.9.18).

Papoulias, S.A., Grossmann, I.E., 1983. A structural optimization approach in process synthesis—II: Heat recovery networks. Comput. Chem. Eng. 7, 707–721. doi:10.1016/0098-1354(83)85023-6.

Pina, E.A., Lozano, M.A., Serra, L.M., 2018. Optimal design of polygeneration systems supported with renewable energy sources and energy storage for a Brazilian hospital, in: Proceedings of ECOS 2018. Guimaraes, Portugal.

Raluy, R.G., Serra, L.M., Guadalfajara, M., Lozano, M.A., 2014. Life cycle assessment of central solar heating plants with seasonal storage. Energy Procedia 48, 966–976. doi:10.1016/j.egypro.2014.02.110.

Ramos, J.C., 2012. Optimización del diseño y operación de sistemas de cogeneración para el sector residencial comercial. PhD Thesis – University of Zaragoza. https://zaguan.unizar.es/record/9901/files/TESIS-2012-136.pdf (accessed 16.11.18).

Rong, A., Lahdelma, R., 2016. Role of polygeneration in sustainable energy system development challenges and opportunities from optimization viewpoints. Renew. Sustain. Energy Rev. 53, 363–372. doi:10.1016/j.rser.2015.08.060.

Rupp, R.F., Lamberts, R., 2017. Fatores de conversão de energia elétrica e térmica em energia primária e em emissões de dióxido de carbono a serem usados na etiquetagem de nível de eficiência energética de edificações [In Portuguese]. http://cb3e.ufsc.br/sites/default/files/RI_61_2017_RelatorioFatoresDeConversaoEnergiaEletricaTermica_EnergiaPrimaria_EmissoesCO2_paraPBEEdifica%20%28corrigido%29_0.pdf (accessed 16.11.18).

Santo, D.B., 2014. An energy and exergy analysis of a high-efficiency engine trigeneration system for a hospital: A case study methodology based on annual energy demand profiles. Energy Build. 76, 185–198. doi:10.1016/j.enbuild.2014.02.014.

Schrage, L., 1999. Optimization modeling with LINGO. Lindo Systems.

Serra, L.M., Lozano, M.A., Ramos, J., Ensinas, A. V., Nebra, S.A., 2009. Polygeneration and efficient use of natural resources. Energy 34, 575–586. doi:10.1016/j.energy.2008.08.013.

Wagner, M.J., Gilman, P., 2011. Technical manual for the SAM physical trough model, NREL/TP-55 Technical report. https://www.nrel.gov/docs/fy11osti/51825.pdf (accessed 16.11.18).

World Energy Council [WEC], 2016. World Energy Resources: Solar 2016. World Energy Counc. https://www.worldenergy.org/wp-content/uploads/2013/10/WER_2013_8_Solar_revised.pdf (accessed 6.9.18).

Yokoyama, R., Shinano, Y., Taniguchi, S., Ohkura, M., Wakui, T., 2015. Optimization of energy supply systems by MILP branch and bound method in consideration of hierarchical relationship between design and operation. Energy Convers. Manag. 92, 92–104. doi:10.1016/j.enconman.2014.12.020.